

Numerical Observation of Three-Dimensional Wing Cracking of Cracked Chevron Notched Brazilian Disc Rock Specimen Subjected to Mixed Mode Loading

N. W. Xu¹ · F. Dai¹ · M. D. Wei¹ · Y. Xu¹ · T. Zhao¹

Received: 17 November 2014 / Accepted: 4 March 2015 / Published online: 15 March 2015
© Springer-Verlag Wien 2015

Abstract The cracked chevron notched Brazilian disc (CCNBD) specimen has been suggested by International Society for Rock Mechanics for measuring mode I fracture toughness of rocks. Subsequently, this specimen geometry has been widely extended to conduct mixed mode fracture tests on rocks as well. A straight through crack front during the fracturing process upon the root of the chevron notch is assumed in the testing principle, but has never been thoroughly evaluated before. In this study, for the first time, the progressive rock fracture mechanism of the CCNBD rock specimen under mixed mode loading is numerically simulated. Specimens under representative mixed mode loading angles are modelled; and the assumption of the straight through crack front growth is critically assessed. The results show that not only the notch tip but also the saw-cut chevron notch cracks during the experiments, yielding a prominent twisted front, far from being straight. The crack front never grows up to the root of the notch ligament and the straight through crack front assumption is never satisfied in the realistic rock fracture progress of this chevron notched specimen subjected to mixed mode loads. In contrast, the fracture progress features typical three-dimensional wing cracking towards the loading ends. The numerically observed progressive fracture mechanism reveals that the measuring principle of mixed mode fracture tests employing CCNBD specimens is significantly violated and the measures of both modes I and II fracture toughness are uncertain.

Keywords Progressive fracture · CCNBD · Mixed mode · Wing crack · Acoustic emission

1 Introduction

Brittle fracture frequently occurs in a variety of geophysical processes and engineering applications involving rocks, such as earthquakes, rockbursts, hydro-fracturing, explosive fracturing, rock cutting, underground excavation and rock slope stability (Chen et al. 2008). In the framework of linear elastic fracture mechanics, rock fracture mechanics has been established to study brittle fracture of rocks, which was essentially extended from the Griffith theory and Irwin's modification of recognizing the significance of stress intensity factor (SIF) at a local crack tip.

Fracture toughness, which describes the capability of a material containing a crack to resist further fracturing, is one of the most important properties of a material for many design applications. Depending on the applied stress experienced by a crack, there are three basic fracture modes: mode I (the tension or opening mode), II (the in-plane shear mode) and III (the tearing mode or out of plane mode) (Anderson 2005). Most studies on the fracture toughness of rocks were focused on mode I since the opening mode failure is frequently encountered (Dai and Xia 2013). International Society for Rock Mechanics (ISRM) also recommended short rod (SR) method and chevron bending (CB) method in 1988 (Ouchterlony 1988), cracked chevron notched Brazilian disc (CCNBD) method in 1995 (Fowell 1995) and very recently semi-circular bend (SCB) method (Zhou et al. 2012; Kuruppu et al. 2014) to measure the mode I fracture toughness of rocks.

However, actual crack propagation in rock mass occurs not only in tension but also in shear (Funatsu et al. 2014). As

✉ F. Dai
fengdai@scu.edu.cn

¹ State Key Laboratory of Hydraulics and Mountain River Engineering, College of Water Resources and Hydropower, Sichuan University, Chengdu 610065, Sichuan, China

is known that in tough ductile materials the mixed mode I/III crack propagation often occurs (Gao and Shih 1998), while in brittle material such as rocks the mixed mode I/II crack propagation is more common (Whittaker et al. 1992). Thus, the critical SIFs in mixed mode (I/II) and pure mode II are crucial to understand the realistic fracturing behaviour of rocks. Many methods with special sample geometries have been developed in the literature for measuring the mixed mode (i.e. modes I and II) and pure mode II fracture toughness of rocks, among which the semi-circular bend (SCB) specimen (Chong and Kuruppu 1988; Lim et al. 1994a, b; Aliha et al. 2010, 2012; Ayatollahi and Aliha 2007) and cracked straight through Brazilian disc (CSTBD) specimen (Awaji and Sato 1978; Atkinson et al. 1982; Ayatollahi and Aliha 2007; Alshayea et al. 2000; Aliha et al. 2010, 2012; Ghazvinian et al. 2013; Haeria et al. 2014) are frequently reported. Recently, ISRM also proposed a suggested method to determine the mode II fracture toughness of rocks using the punch-through shear (PTS) specimen (Backers and Stephansson 2012). Employing these designed sample geometries and experimental implementations, the laboratory testing of rock fracture toughness in terms of the ratio of mode II fracture toughness (K_{IIc}) to mode I fracture toughness (K_{Ic}) at the local scale can be determined using analytical or numerical methods with experimental recorded critical loads as input.

The CCNBD method has received wide acceptance in the research realm of rock fracture mechanics due to its many advantages over other conventional testing schemes involving easier sample preparation, much higher failure loads, simpler testing procedure, lower scatter of test results, and a wide range of specimen geometries that can be tested (Fowell and Xu 1994). Another distinct merit of the CCNBD specimen is its easy adaptation for mode II or mixed mode fracture tests (Chang et al. 2002). Some selected publications about the use of the CCNBD specimen on mixed mode fracture researches include Chang et al. (2002), Ayatollahi and Aliha (2008), Amrollahi et al. (2011), Erarslan and Williams (2013) and Aliha and Ayatollahi (2014). A recent review on the mixed mode experimental results (Ayatollahi and Aliha 2008) depicts that data obtained using CCNBD specimens on Keochang Granite and Yeosan Marble (Chang et al. 2002) scatter significantly compared with those from other samples with a pre-fabricated straight through crack (Awaji and Sato 1978; Khan and Al-Shayea 2000). Apart from the size effects (Bažant 2000) on measures, it is noted that for mixed mode fracture tests using CCNBD specimens (Ayatollahi and Aliha 2008; Amrollahi et al. 2011; Aliha and Ayatollahi 2014), a straight through crack front growth (Ouchterlony 1988; Chang et al. 2002) up to the root of the chevron notch is assumed; this assumption has been widely adopted to determine the critical modes I and II SIFs and thus the corresponding mixed mode fracture toughness

values. However, this assumption has never been thoroughly evaluated yet; and this might induce severe data scatter in experiments.

In this study, a numerical code RFPA3D is adopted to numerically simulate the progressive fracture process of the CCNBD rock specimen subjected to mixed mode loading. The PFPA3D code is employed because of its merit of realistically simulating the failure process considering the heterogeneity of rock materials using the Weibull distribution (Tang and Kaiser 1998) and the acoustic emissions (AE) associated with microcracking can be numerically attained. This paper is organized as follows. In Sect. 2, the traditional principle of the CCNBD method for mixed mode fracture tests is introduced and the postulations are schematically presented. Section 3 briefly describes the RFPA3D code and setups of the numerical model, followed by the simulated progressive fracturing process of the specimen in Sect. 4. A comprehensive discussion on the fracture mechanism is given in Sect. 5 and the conventional measuring principle of the mixed mode rock fracture toughness is challenged. Section 6 summarizes the whole studies.

2 The Principle of CCNBD Method and its Postulation

A schematic of the CCNBD sample geometry under mixed mode loading is shown in Fig. 1, where P is the applied load during the test; B is the thickness of the CCNBD disc; R is the radius of the disc specimen; a is the crack length and α , the dimensionless crack length ($\alpha = a/R$); a_0 is the initial chevron notched crack length ($\alpha_0 = a_0/R$); a_1 is the final chevron notched crack length ($\alpha_1 = a_1/R$); a_m is the critical crack length ($\alpha_m = a_m/R$); α_B is the dimensionless thickness ($\alpha_B = B/R$).

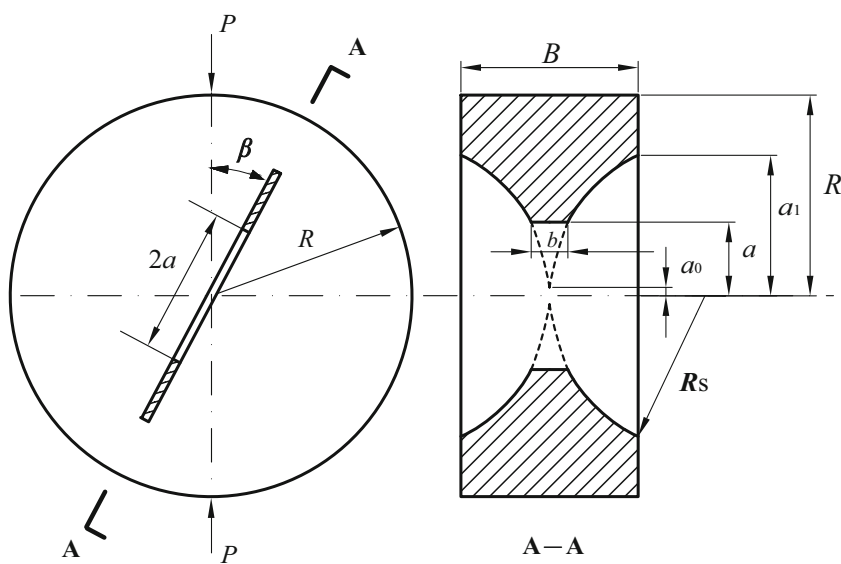
If the loading angle β equals to zero, Fig. 1 depicts the ISRM suggested CCNBD method for mode I fracture toughness measurement (Fowell 1995). The mode I SIF of a crack at length a (dimensionless crack length of α) can be calculated using Eq. (1). The mode I fracture toughness can then be calculated by Eq. (2).

$$K_I = \frac{P}{B\sqrt{R}} Y^* \quad (1)$$

$$K_{IC} = \frac{P_{\max}}{B\sqrt{R}} Y_{\min}^* \quad (2)$$

where K_I is the mode I SIF of the fracture sample; K_{IC} is the mode I fracture toughness of rock material; P_{\max} is the peak load at failure; Y^* is the dimensionless SIF of the disc specimen and Y_{\min}^* is the critical dimensionless SIF of Y^* , which corresponds to the failure load recorded during testing.

Fig. 1 Geometry and the mixed mode loading of a CCNBD specimen



For the fracture tests of CCNBD specimens under mixed mode loading, no suggested methods are proposed by the ISRM to determine the mixed mode SIF. Some researchers have attempted this issue by adopting the straight through crack front assumption (Ouchterlony 1988). Shetty et al. (1985) proposed the SIF solutions for CSTBD specimen with a straight through crack length of $2a$.

$$\begin{cases} K_I = \frac{P}{\pi RB} \sqrt{\pi a} N_I = \frac{P}{\sqrt{\pi RB}} \sqrt{\alpha} N_I \\ K_{II} = \frac{P}{\pi RB} \sqrt{\pi a} N_{II} = \frac{P}{\sqrt{\pi RB}} \sqrt{\alpha} N_{II} \end{cases} \quad (3)$$

where P is the compressive load and a is the half crack length. N_I and N_{II} are the dimensionless SIF, dependent on the dimensionless half crack length α (a/R) and the loading angle β . The approximate solutions for N_I and N_{II} with the applicable equations are documented by Atkinson et al. (1982), Shetty et al. (1985) and Fowell and Xu (1994).

Employing the straight through crack front assumption (Ouchterlony 1988), Chang et al. (2002) developed the governing equations of the SIFs for CCNBD specimen under mixed mode loading, by substituting B in Eq. (3) to $B \times \sqrt{(\alpha - \alpha_0) / \sqrt{(\alpha_1 - \alpha_0)}}$. It is assumed by Chang et al. (2002) that the crack front width increases linearly from zero to B as the dimensionless crack length increases from α_0 to α_1 .

$$\begin{cases} K_I = \frac{P}{\sqrt{\pi RB}} \sqrt{\alpha} \sqrt{\frac{\alpha_1 - \alpha_0}{\alpha - \alpha_0}} N_I \\ K_{II} = \frac{P}{\sqrt{\pi RB}} \sqrt{\alpha} \sqrt{\frac{\alpha_1 - \alpha_0}{\alpha - \alpha_0}} N_{II} \end{cases} \quad (4)$$

Note that the measuring principle of the CCNBD method under mixed mode loading postulates that the primary fracture initiates from the tip of the jag notch and grows symmetrically towards both loading ends with

perfect straight-line crack fronts, as shown in Fig. 2. The A, B, C and D in Fig. 2e correspond to four typical progressive fracture stages in Fig. 2a–d, respectively. During the stable fracture propagation, the crack front increases from zero to B as the dimensionless crack length increases from α_0 to α_1 . When the loading force P reaches its maximum of P_{max} (C point in Fig. 2e), the fracture is assumed to grow to the root of the notch ligament (Chang et al. 2002) and the CCNBD specimen appears to be a CSTBD specimen. The mixed mode fracture test of a CCNBD specimen turns into a typical CSTBD fracture test under mixed mode loading; and the corresponding modes I and II SIFs and fracture toughness values can thus be calculated via Eq. (4) by virtue of the experimentally recorded peak force P_{max} and the N_I and N_{II} solutions commonly derived independently via numerical tools before performing the experiments.

3 Brief Description of RFPA3D and Model Setup

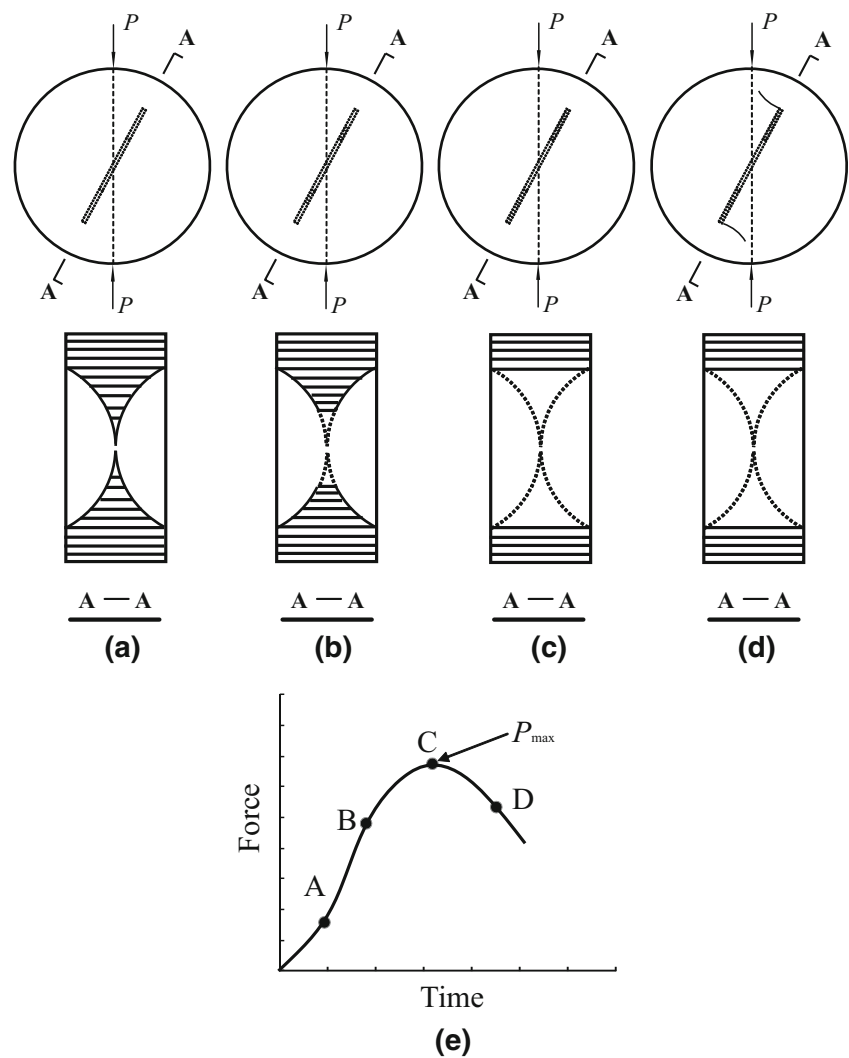
3.1 The RFPA3D Code

The RFPA code was developed by Tang (1997) to more clearly simulate the progressive failure of brittle materials containing initial random distribution of micro-features. To statistically consider the variability of the bulk strength, the mechanical parameters of the model elements are assumed to follow a Weibull distribution (Weibull 1939) in this code.

$$W(x) = \frac{m}{x_0} \left(\frac{x}{x_0}\right)^{m-1} \exp\left[-\left(\frac{x}{x_0}\right)^m\right] \quad (5)$$

where m defines the shape of the Weibull distribution function, referred to the homogeneity index, x is the

Fig. 2 Fracture principle and assumption of a CCNBD specimen under mixed mode loading (Chang et al. 2002)



mechanical parameter of an element, x_0 is the even value of the parameter of elements. According to the Weibull distribution, the larger the m value the more the mechanical properties of the elements approach the mean value, i.e. a more homogeneous rock specimen (Liang et al. 2012).

Compared with traditional numerical tools, the RFPA code and its 3D extension RFPA3D have two significant features (Tang 1997). First, by introducing heterogeneity of rock properties into the model, the code can simulate the nonlinear deformation of a quasi-brittle material with an ideal brittle constitutive law at the local scale. Second, by quantitatively reducing material parameters of failed elements, the code can simulate discontinuum mechanics issues within the framework of continuum mechanics. Details of the RFPA3D code can be found elsewhere (Liang et al. 2012). The robustness of this code in simulating rock fracture or failure has been evaluated by numerous studies involving the failure mechanism of rock specimens (Erarslan et al. 2012; Tang 1997; Tang and

Kaiser 1998; Wei et al. 2015), three-dimensional rock fracture initiation and growth (Liang et al. 2012; Wang et al. 2014) and stability analysis of rock slope and underground caverns in hydropower stations (Xu et al. 2012, 2014, 2015).

The well-known Mohr–Coulomb failure criterion with a tensile cut-off is used as the damage constitutive model in RFPA3D (Liang et al. 2012). Tensile failure occurs in the elements as long as the minimum principal stress of an element reaches the uniaxial tensile strength. The evolution of tensile damage can be expressed as follows:

$$D = \begin{cases} 0 & (\varepsilon < \varepsilon_{t0}) \\ 1 - \frac{\sigma_{rt}}{\varepsilon E_0} & (\varepsilon_{t0} \leq \varepsilon \leq \varepsilon_{ut}) \\ 1 & (\varepsilon > \varepsilon_{ut}) \end{cases} \quad (6)$$

where σ_{rt} is the residual strength of an element, E_0 is the elastic modulus of the undamaged material, ε is the tensile strain, ε_{t0} is the threshold value of the minimum principal

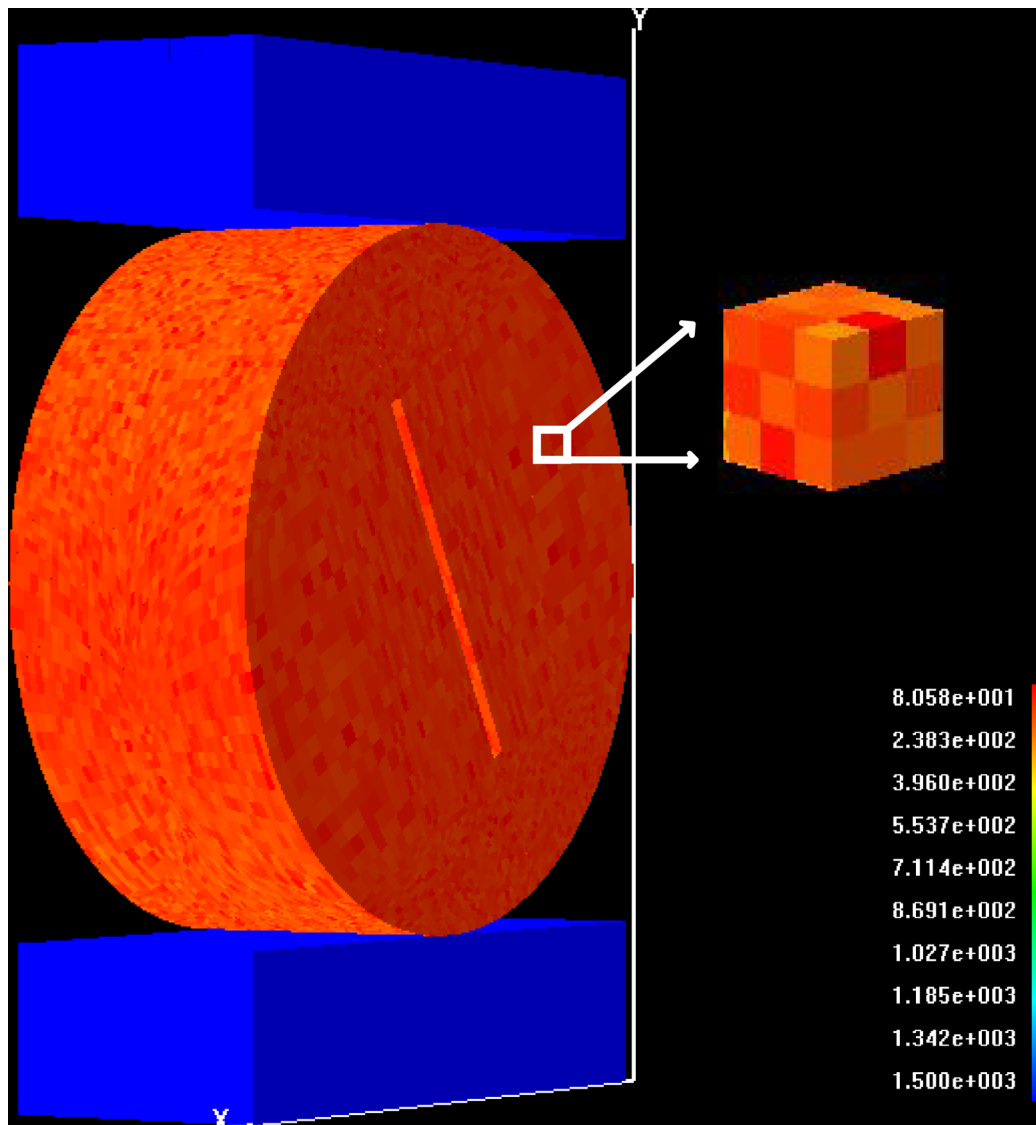


Fig. 3 Three-dimensional numerical model of a CCNBD specimen ($\beta = 28^\circ$)

strain when tensile damage occurs and ε_{ut} is the threshold value of the minimum principal strain when the elements detach. The Mohr–Coulomb failure criterion is employed to define the shear damage of an element and the evolution of shear damage can be expressed as:

$$D = \begin{cases} 0 & (\varepsilon_1 < \varepsilon_{c0}) \\ 1 - \frac{\sigma_{rc}}{E_0 \varepsilon_1} & (\varepsilon_1 \geq \varepsilon_{c0}) \end{cases} \quad (7)$$

where ε_1 is the maximum compressive principal strain, ε_{c0} is the threshold strain as shear damage occurs, σ_c is the uniaxial compressive strength of an element, σ_{rc} is the residual strength of an element and $\sigma_{rc} = \kappa \sigma_c$ (κ represents the residual strength coefficient). In the processes of damage evolution, the resistance load capability of the elements gradually decreases and the elements maintain a

certain residual strength after the failure criterion can be reached. Although only uniaxial compressive and tensile strain damage are introduced above, the effect of the other two principal stresses on the maximum principal strain or the minimum principal strain under three-dimensional stress conditions has also been considered. The equivalent strain method is employed as follows:

$$\bar{\varepsilon} = \sqrt{\langle \varepsilon_1 \rangle^2 + \langle \varepsilon_2 \rangle^2 + \langle \varepsilon_3 \rangle^2} \quad (8)$$

where,

$$\langle \varepsilon_i \rangle = \begin{cases} \varepsilon_i & (\varepsilon_i \leq 0, \quad i = 1, 2, 3) \\ 0 & (\varepsilon_i > 0, \quad i = 1, 2, 3) \end{cases} \quad (9)$$

As a failed element releases its stored elastic energy, the failed or damaged element is assumed to be an acoustic

emission (AE) source (Tang 1997). The AE counts assumed to be proportional to the number of damaged elements and the strain energy released by damaged elements

are recorded. Following above assumptions, the RFPA3D can simulate the AE activities including the AE counts and the cumulative AE energy release. The accumulative damage, denoted as D , can be counted using the following equation:

$$D = \frac{\sum_{i=1}^s n_i}{N} \tag{10}$$

where s is the number of calculation steps, n_i is the number of damaged elements in the i th step and N is the total number of elements in the model.

3.2 Model Setup

Five CCNBD specimen configurations under mixed mode loading angle of 28° , 30° , 33° , 45° and 70° are simulated. All specimens satisfy the dimensional requirements of the ISRM suggested CCNBD specimens (Fowell 1995) for a valid range of geometries for fracture toughness measures. The radius of the disc (D) is 32 mm and the thickness (B) is 25 mm. The saw radius (R_S) for preparing the chevron notch is 20 mm, the initial chevron notched crack length

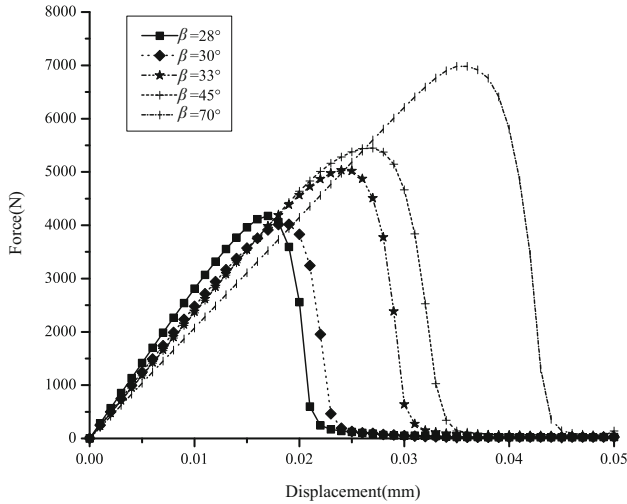


Fig. 4 The numerically simulated force–displacement curves of the CCNBD tests under mixed mode loading ($\beta = 28^\circ$, 30° , 33° , 45° and 70°)

Fig. 5 The simulated failure patterns of CCNBD specimens under mixed mode loading: minimum principal stress distribution on the sample surface

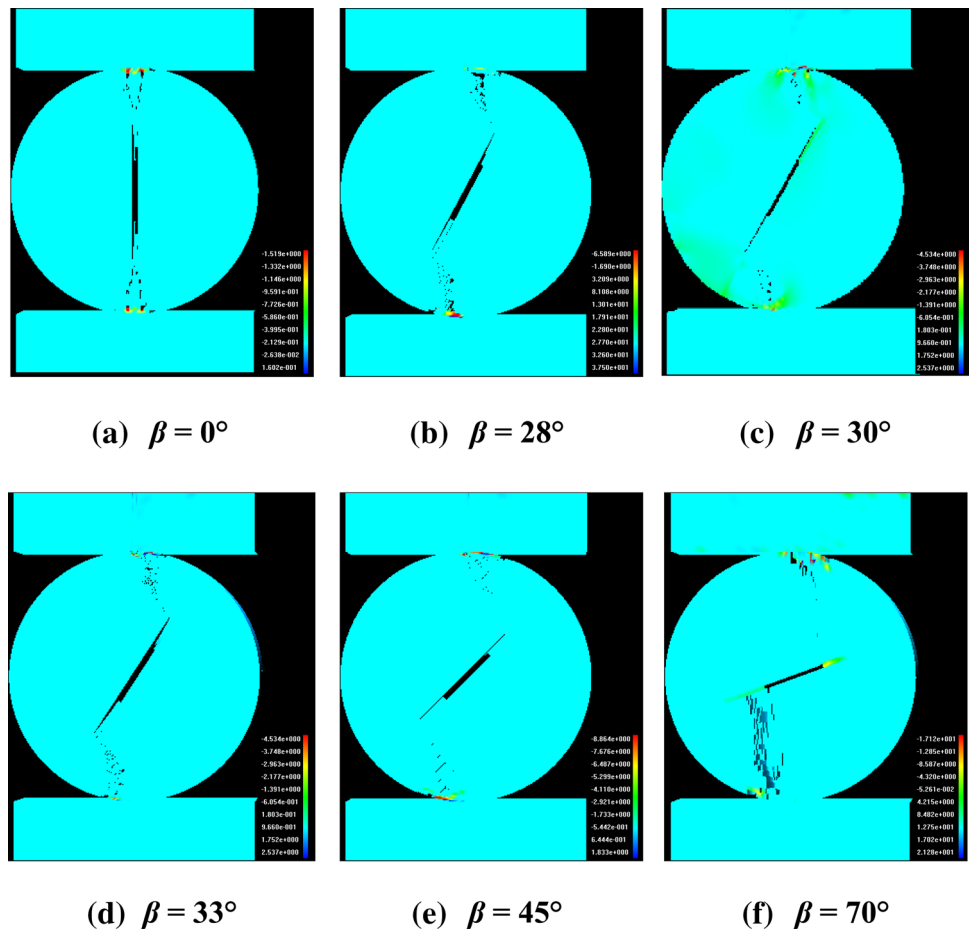
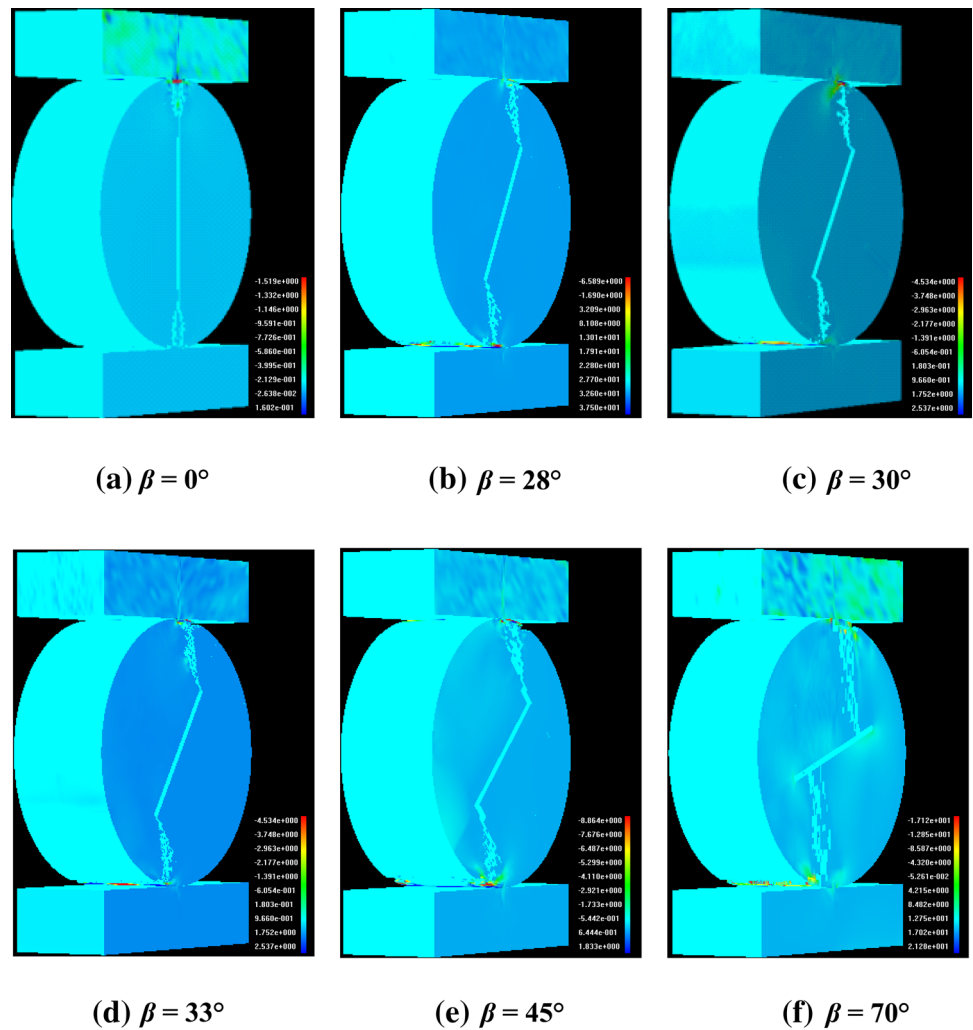


Fig. 6 The numerically simulated failure patterns of CCNBD specimens under mixed mode loading: minimum principal stress distribution from stereo viewpoint ($\beta = 28^\circ$)



(a_0) is 8 mm, and the final chevron notched crack length (a_1) is 18 mm. All dimensions are converted to dimensionless parameters as follows: $\alpha_0 = a_0/R = 0.25$, $\alpha_1 = a_1/R = 0.5625$, $\alpha_B = B/R = 0.7810$, $\alpha_S = R_S/R = 0.625$.

Figure 3 shows the numerical CCNBD model subjected to a mixed mode loading angle of 28° with a typical three-dimensional hexahedral element distribution. The model is meshed using 168,960 elements. The simulated sandstone is relative homogenous with m , the homogeneity index in Eq. (5), taken as 10. Mean Young’s modulus of 60 GPa, Poisson’s ratio of 0.25, tensile strength of 9.9 MPa and uniaxial compressive strength of 100 MPa, are measured from samples cored from sandstone blocks, directly obtained from quarries (Dai et al. 2015). The loading steel platens are rigid. To mimic real experiments, a displacement control of 0.001 mm per step is applied vertically to the top platen and the bottom platen is fixed. A low displacement loading facilitates stable crack growth associated with microcracking throughout the fracturing process

in the actual experiments. The force–displacement curve can be numerically recorded similar to that in a real laboratory experiment.

4 Numerical Results

4.1 Progressive Fracture of CCNBD Specimens with Loading Angles β of 28° , 30° , 33° , 45° and 70°

Figure 4 shows the numerically simulated force–displacement curves of the CCNBD test with mixed mode loading angles of 28° , 30° , 33° , 45° and 70° . All the simulated force–displacement curves feature a low rising part up to the peak force and then a rather steep decreasing post-failure part, comparable to the force–displacement curves from typical rock fracture experiments (Cui et al. 2010). According to the measuring principle (Chang et al. 2002),

Fig. 7 Photo of recovered CCNBD samples under mixed mode loading (reproduced after Erarslan and Williams 2013)

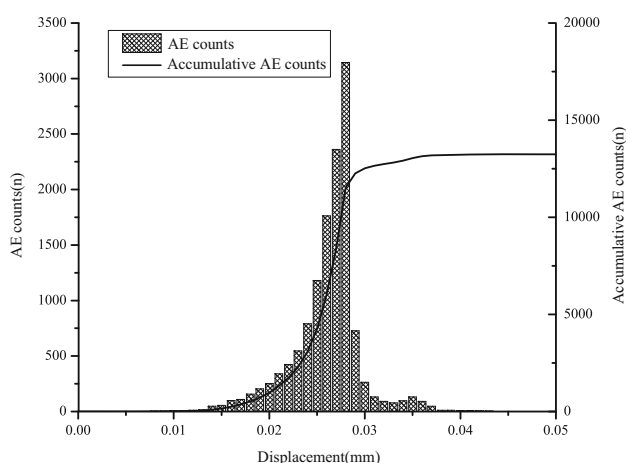


Fig. 8 Simulated AE counts and accumulated AE counts during the failure process of the CCNBD test with a mixed loading angle of $\beta = 28^\circ$

the turning point (i.e. the point at the peak force) on the force–displacement curve denotes that the primary fracture grows up to the root of the notch ligament and the CCNBD specimen turns into a standard CSTBD specimen.

The failure processes of CCNBD specimens under different mixed mode loading cases (loading angle β of 28° , 30° , 33° , 45° and 70°) are simulated, which are shown by the minimum principal stress distributions of the front cross section (Fig. 5, sample surface) and from a stereo point of view (Fig. 6). For comparison purposes,

the failure pattern under mode I loading case ($\beta = 0^\circ$) is also simulated and included in Figs. 5 and 6. The different loading angles induce different stress states, the ratio of the modes I and II SIF of the crack are different and thus the fracture propagations are distinct. It is evident from Figs. 5 and 6 that except for the pure mode I loading case ($\beta = 0^\circ$), in which the primary fracture initiates and develops approximately within the original notched plane, the fractures in other five mixed loading cases deviate from the chevron notched plane in different extent and finally approach the top and bottom loading ends. All fracture propagations of CCNBD specimens with loading angle β of 28° , 30° , 33° and 45° depict typical wing cracking; and the larger the loading angle β , the larger the deflected angle by which the fracture kinks. As the loading angle β increases up to 70° , the simulated fracture pattern differs dramatically from other four loading cases. As shown in Figs. 5f and 6f, the initiation of the main fracture is not from the crack tip, but somewhere near the centre of the disc with a large deflected angle. The damaged region is much wider and scattered compared with other mixed mode loading cases (i.e. $\beta = 28^\circ$, 30° , 33° and 45°).

The simulated fracture patterns and their development on the sample surface (Figs. 5, 6) for all five mixed mode loading cases are comparable to those reported by Erarslan and Williams (2013) from physical experiments (Fig. 7). Note that conventional laboratory fracture tests on CCNBD specimens can record the force–displacement history or

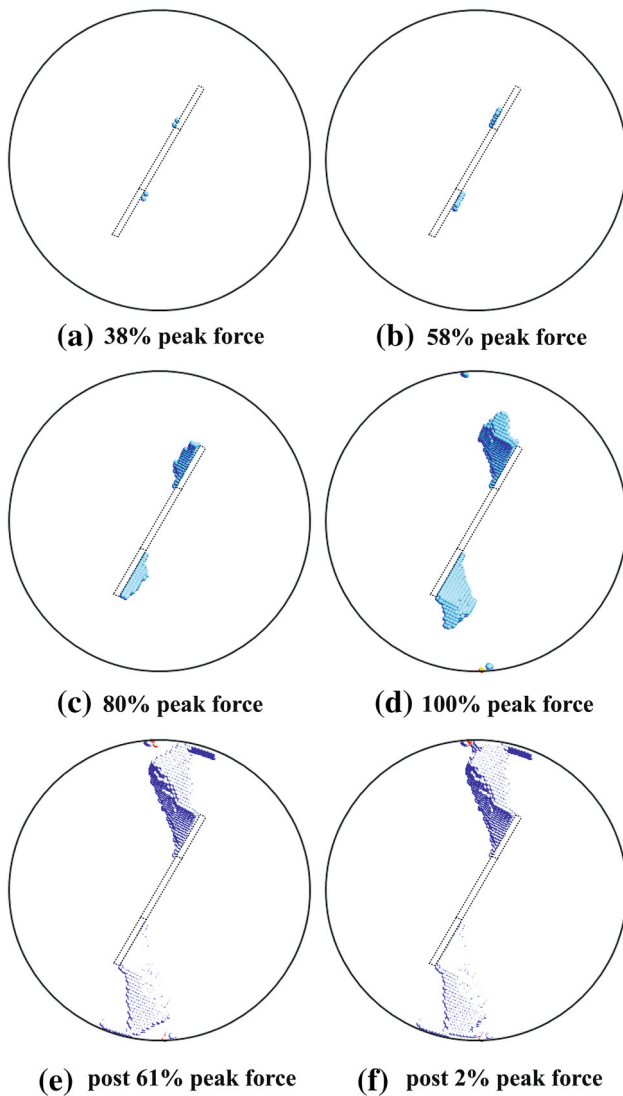


Fig. 9 The numerically simulated failure process of the CCNBD specimen under mixed mode loading: AE distribution in the view of the direction perpendicular to the sample surface ($\beta = 28^\circ$)

even the crack surface displacement field via advanced techniques (e.g. digital image correlation); however, in general, only the fracture patterns on the sample surface can be visualized, while the inner crack emanation and development can hardly be observed and understood. This scenario is especially severe for a specimen with three-dimensional fracture configurations (e.g. CCNBD specimen). Under such given circumstances, numerical tools are effective to trace the progressive failure process of the CCNBD specimen under mixed mode loading and to uncover the fracture mechanism beneath the sample surface. To demonstrate this, CCNBD fracture tests with two typical loading angles ($\beta = 28^\circ$ and 70°) are simulated and the progressive fracture inside the specimens is discussed in the following sub-sections.

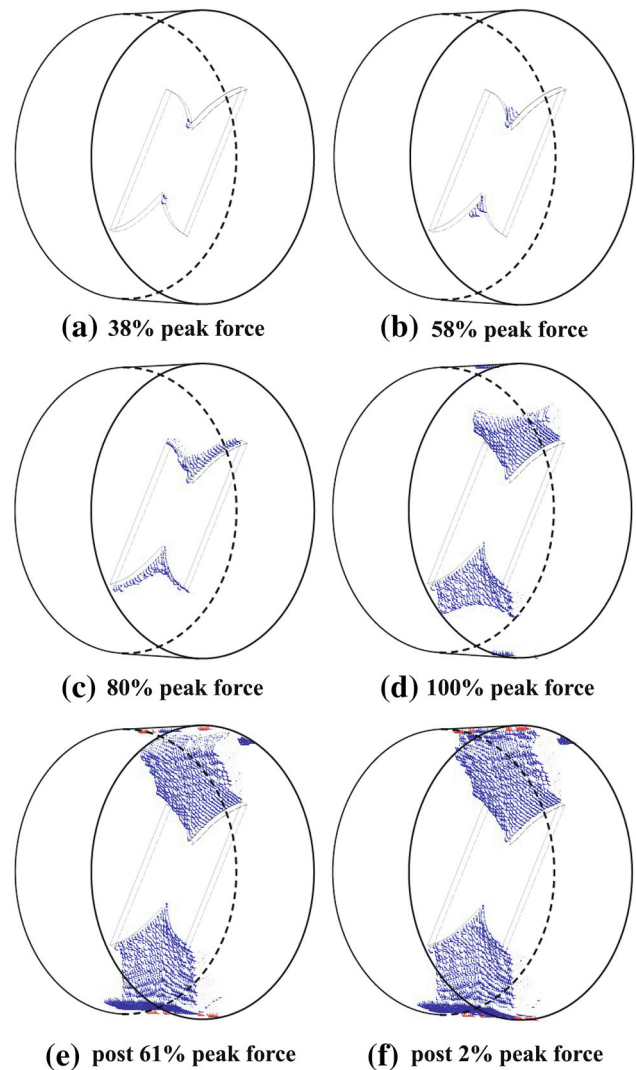
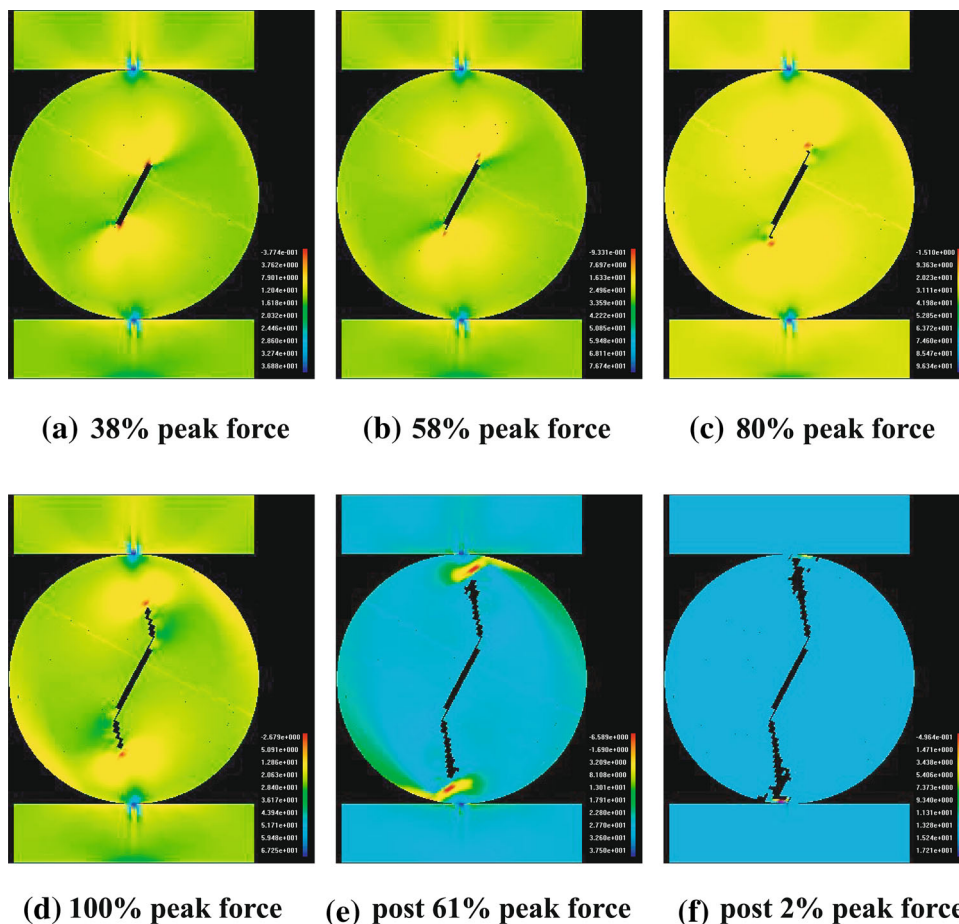


Fig. 10 The numerically simulated failure process of the CCNBD specimen under mixed mode loading: AE distribution from stereo viewpoint ($\beta = 28^\circ$)

4.2 Progressive Fracture of CCNBD Specimen with a Loading Angle of 28°

Figure 8 shows the associated AE counts and accumulated AE counts during the simulated failure process of the CCNBD test with a mixed loading angle of $\beta = 28^\circ$; the force–displacement curve can be seen in Fig. 4. The numerically simulated progressive failure of a CCNBD specimen under mixed mode loading ($\beta = 28^\circ$) can be visualized through AE distribution during six typical loading stages, i.e. 38 % peak force, 58 % peak force, 80 % peak force, 100 % peak force, post 61 % peak force and post 2 % peak force, viewing in the direction perpendicular to the sample surface (Fig. 9) and in a stereo viewpoint (Fig. 10). The blue and red circles of AE distribution denote the tensile and shear failure of the

Fig. 11 The simulated fracture process of the CCNBD specimen under mixed mode condition ($\beta = 28^\circ$): minimum principal stress distribution of the central cross section through the notch tip



elements, respectively. It is evident that the AE distribution in circles (Figs. 9, 10) is dominantly in blue, denoting tensile damage. The red circles, i.e. the shear damage, occur only at both loading contacts as the bearing force is up to 100 % peak force, which reveals that the fracturing of the central notched region is primarily in tension upon failure. The shear damage is only induced by the three-dimensional stress effects at the contact region of the disc with loading platens.

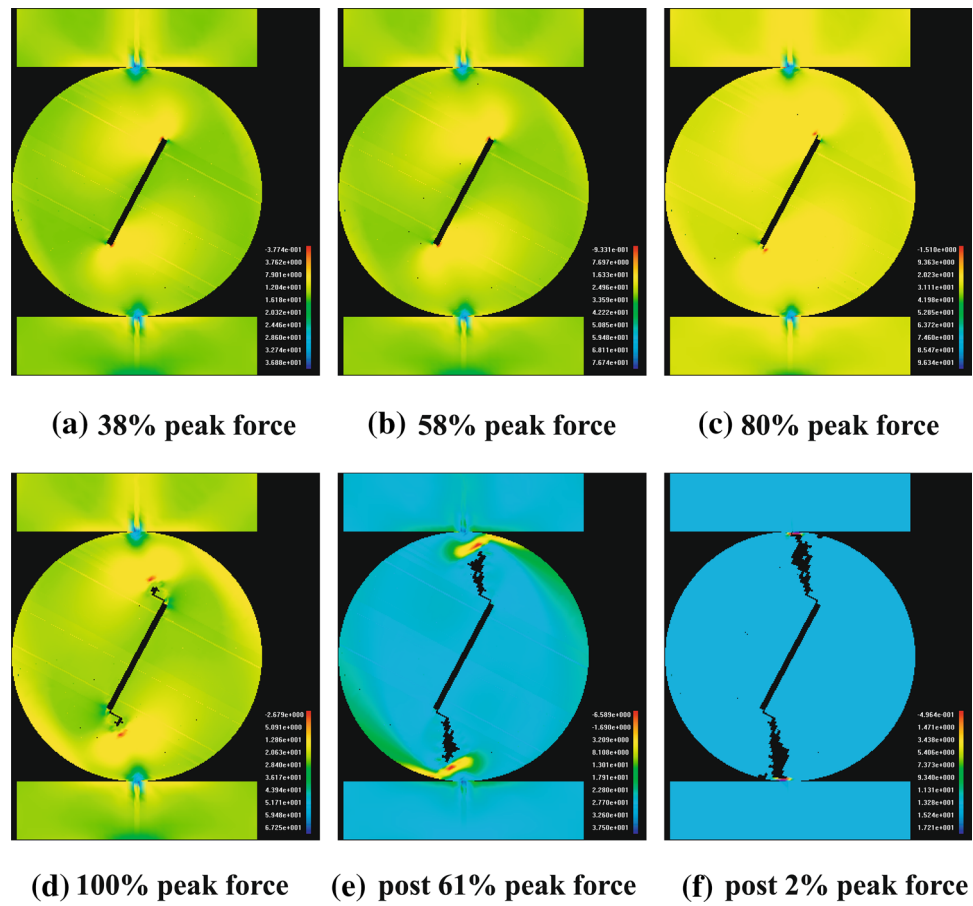
Due to the stress concentration at the local scale, the special fabricated chevron notch does facilitate the crack emanation from the notch tip, as evidenced by the AE events at the loading stage I (38 % peak force). Through loading stages I (38 % peak force) to II (58 % peak force), cracks grow further along the plane of the notch ligament, appearing to be self-similar (Fig. 9). After stage II (58 % peak force), cracking deviates from the prescript fracturing route of the notch ligament. An inevitable scenario emerging from this stage is that the chevron saw-cut notch is also damaged to some extent from both sides of the tip. From stages III (80 % peak force) to IV (100 % peak force), the fractures grow not only from the notch tip but also from two chevron notched edges and develop

significantly. The growing crack front is far from being straight within the plane of the notch ligament but considerably curved and twisted in space, approaching the two loading ends. The post-failure stages V (post 61 % peak force) and VI (post 2 % peak force) depict that the specimen gradually loses its load-bearing capability.

Special attention should be paid on the critical or the peak loading stage (i.e. stage IV), at which stage the necessary information involving the dimensionless crack length and crack front shape can be determined for calculating both the critical modes I and II SIFs, and thus the fracture toughnesses using Eq. (4) in the laboratory fracture tests. Indeed, the realistic crack front at this critical stage is not confined to the notched plane, and not straight through at all but significantly twisted in a three-dimensional fashion; and this completely violates the measuring assumption (Chang et al. 2002) for mixed mode fracture toughness determination via CCNBD specimens.

To clearly interpret the twisted three-dimensional crack development, the simulated inner fracture process of CCNBD specimen under mixed mode condition ($\beta = 28^\circ$) is revealed by the minimum principal stress distribution at the central cross section through the notch tip (Fig. 11), the

Fig. 12 The simulated fracture process of the CCNBD specimen under mixed mode condition ($\beta = 28^\circ$): minimum principal stress distribution of the cross section through one quarter thickness



cross section through one quarter thickness (Fig. 12) and the cross section through the disc surface (Fig. 13), respectively.

With the width of the cut section thin enough, those figures can be regarded as giving the failure progress of the CSTBD specimen under mixed mode loading. Figures 11, 12 and 13 represent CSTBD specimens with three different crack lengths. The crack length for Fig. 11 is the least one, equal to the length of the minimum crack length a_0 of the CCNBD; and thus minimum principal stress distribution in Fig. 11 can reflect the progressive fracture of the CCNBD sample through the notched tip. The stress concentration at the notch tip is severe. Upon 58 % peak load, the crack tip fractures parallel to plane of the chevron notch. As the load reaches 80 % of the peak force, the fracture starts to deflect and grows up to both loading ends, as shown in Fig. 11c–f, featuring typical two-dimensional wing cracking.

The crack length for Fig. 13 (sample surface) is the longest one, the length of which equals to the maximum crack length a_1 of the CCNBD specimen. The minimum principal stress distribution in Fig. 13 illustrates the progressive fracture of the CCNBD specimen at the notch root. Compared to the fracture progress at the notch tip (Fig. 11), the fracture at the root lags evidently. As the load

increases from 38 % peak force to 58 % peak force and afterwards, no microcrackings occur. Upon 80 % peak force, the stress concentration is visible. From Fig. 13c–e, the fracture emanating from the crack tip does not grow within the notched zone but kinks away from the original crack surface, propagating inside the specimen towards the loading ends until the final catastrophic failure of the specimen occurs as shown in Fig. 13f. Figure 12 shows the crack growth of a CSTBD specimen with the crack length equal to the average crack length of the CCNBD specimen; the fracture characteristics depict the scenario between that of the Figs. 11 and 13. Comparing the cracking developments in all three thin sections, it is evident that microcrackings also occur at the saw-cut chevron edges and that the region near the notch tip cracks prior to those sections far away from the tip.

4.3 Progressive Fracture of CCNBD Specimen with a Loading Angle of 70°

With the increase of the loading angle β , the mode I SIF decreases while the mode II SIF increases (Ayatollahi and Aliha 2007). As the loading angle β is up to 70° , the fracture process of the CCNBD specimen is distinct from

Fig. 13 The simulated fracture process of the CCNBD specimen under mixed mode condition ($\beta = 28^\circ$): minimum principal stress distribution of the cross section on the sample surface

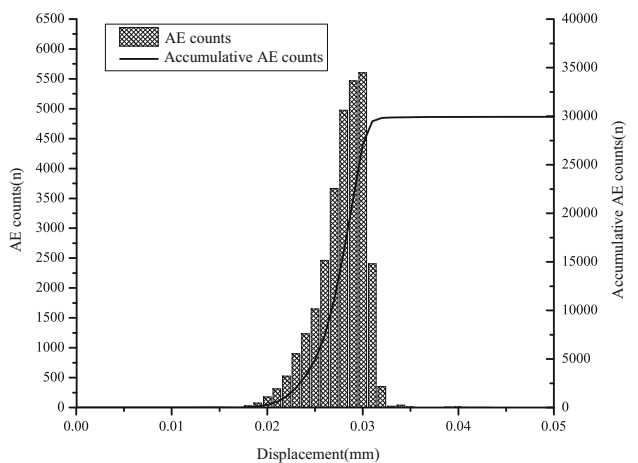
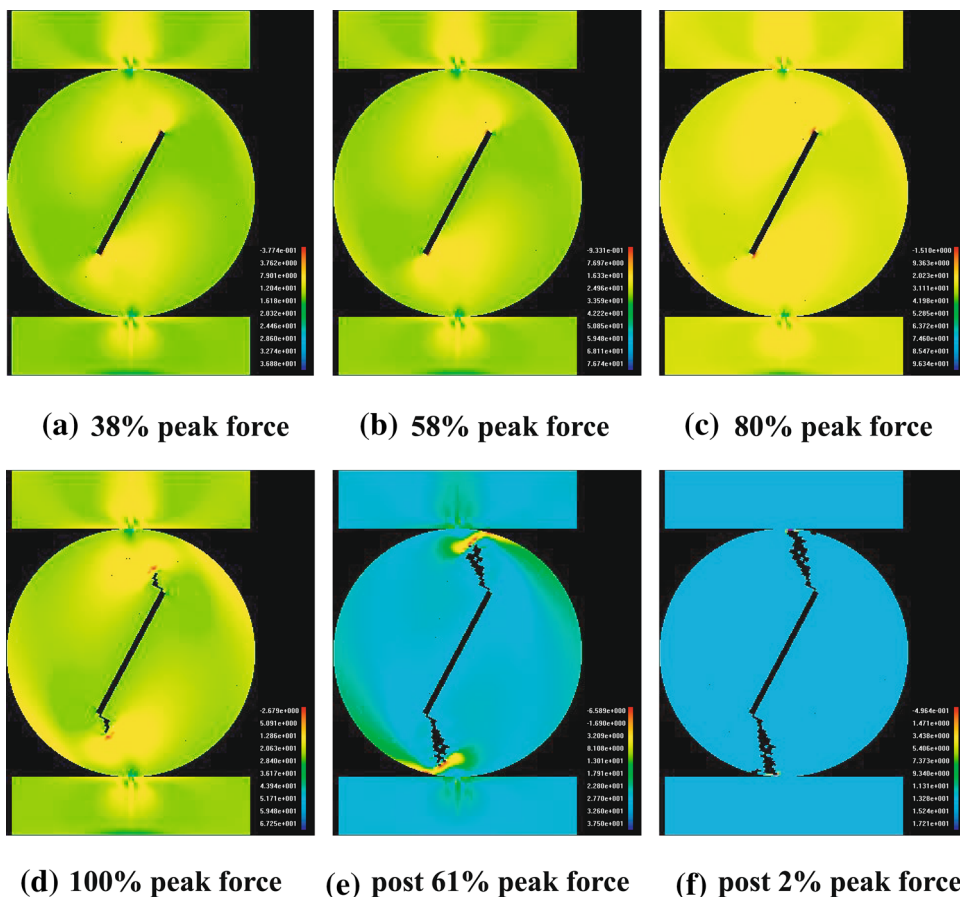


Fig. 14 Simulated AE counts and accumulated AE counts during the failure process of the CCNBD test with a mixed loading angle of $\beta = 70^\circ$

other mixed modes with lower loading angles. Figure 14 shows the associated AE counts and accumulated AE counts during the simulated failure process of the CCNBD test with a mixed loading angle of $\beta = 70^\circ$; the force–displacement curve can be seen in Fig. 4 as well. Compared with Fig. 8, both AE counts and accumulated

AE counts are significantly higher for $\beta = 70^\circ$ than those for $\beta = 28^\circ$, since the bearing force required to fail the specimen is much higher. More details of the progressive fracture process at the given loading angle can be observed through AE events distribution viewing in the direction perpendicular to the sample surface as shown in Fig. 15 and in a stereo viewpoint as given in Fig. 16 ($\beta = 70^\circ$). Six typical loading stages are demonstrated, i.e. 83 % peak force, 92 % peak force, 100 % peak force, post 61 % peak force, post 49 % peak force and post 2 % peak force. Due to the stress concentration, the very first cracking also occurs at the tip of the fabricated chevron notch, as shown by the AE events at the loading stage I (83 % peak force). However, right after that, the pre-fabricated notch has little influence on the further fracture propagation of the specimen. Compared to the loading case with a mixed loading angle of $\beta = 28^\circ$, through loading stages I (83 % peak force) to II (92 % peak force) in Figs. 15 and 16, cracks do not grow along the notched plane but rather deviate from it, growing towards loading ends. From stages III (100 % peak force) to IV (post 61 % peak force), it is featured that the two chevron saw-cut notch edges are also damaged to some extent from both sides. The crack fronts are rather wide and straight

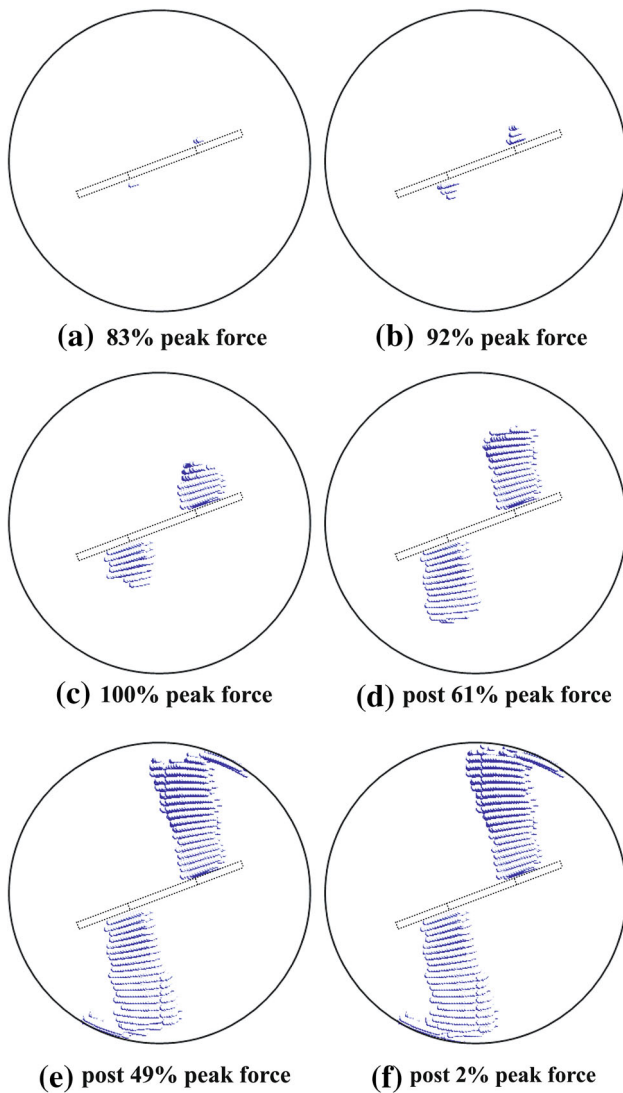


Fig. 15 The numerically simulated failure process of the CCNBD specimen under mixed mode loading: AE distribution in the view of the direction perpendicular to the sample surface ($\beta = 70^\circ$)

(Figs. 15c, d, 16c, d) compared to the loading case with a loading angle of $\beta = 28^\circ$.

Similar to the simulated mixed mode loading case of $\beta = 28^\circ$, the progressive fracture process of the CCNBD specimen under a mixed mode loading angle of $\beta = 70^\circ$ can be illustrated by the minimum principal stress distribution at three thin cross sections parallel to the sample surface: the central cross section through the notch tip (Fig. 17), the cross section through one quarter thickness (Fig. 18) and the cross section through the disc surface (Fig. 19), respectively. Six typical loading stages (namely, 83 % peak force, 92 % peak force, 100 % peak force, post 61 % peak force, post 49 % peak force and 2 % peak force) are demonstrated. It is evident that the fracture initiates from the notch tip (Fig. 17b) and then develops

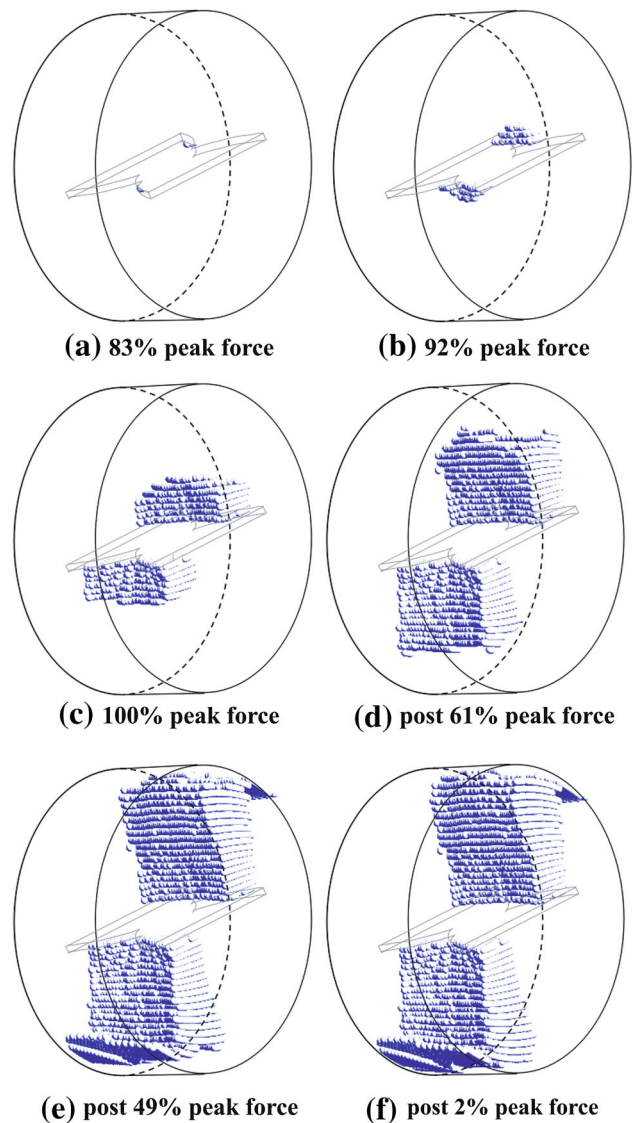
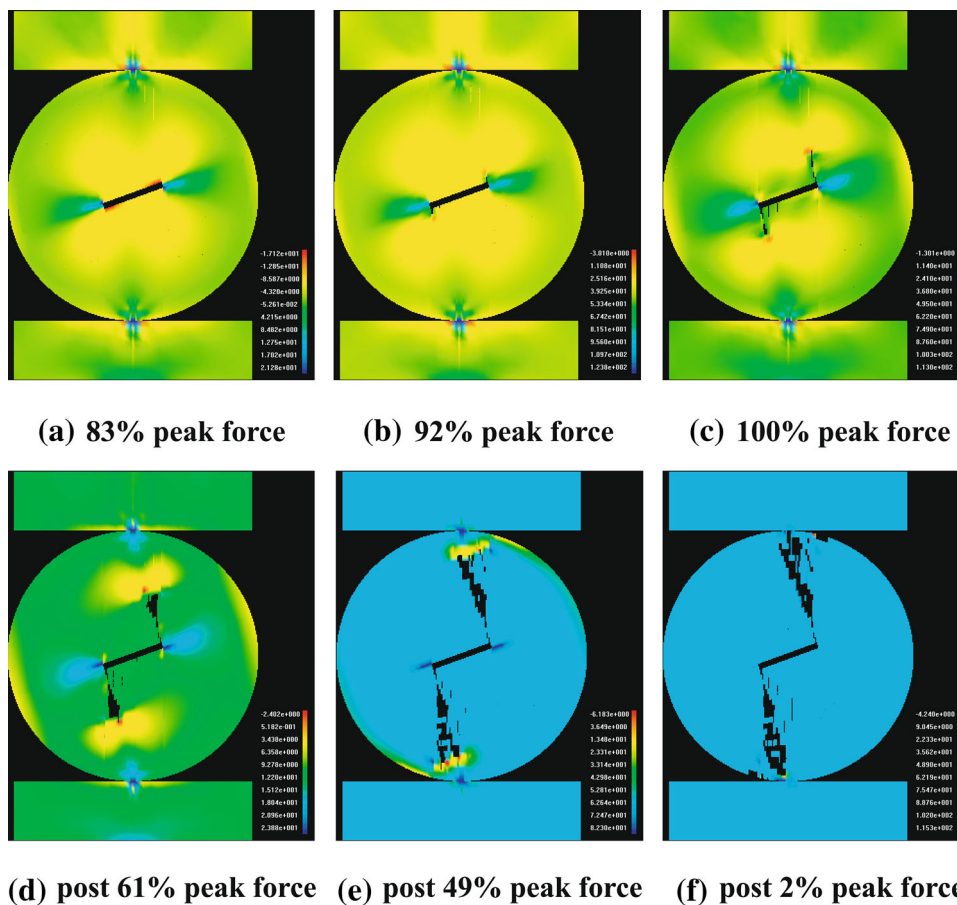


Fig. 16 The numerically simulated failure process of the CCNBD specimen under mixed mode loading: AE distribution from stereo viewpoint ($\beta = 70^\circ$)

almost vertically (Fig. 17b, c). Compared with the mixed mode loading case with $\beta = 28^\circ$ (Fig. 11c–f), the damaged zone is much wider and scattered (Fig. 17c–f). This is due to the much higher loading force required to fail the specimen with a large mixed mode angle (Fig. 4). Both Figs. 18 and 19 show that the crackings at both sections initiate not from the notch tips but from somewhere near the centre of the notch, quite near the tip of the chevron notch. The saw-cut edges of the chevron notch rarely crack, which reveal that under such mixed mode loading circumstances, the failure is dominated by the tension and the cutting edges relatively far away from the notch tip have little influence on the failure of the rock disc. Further cracking is similar to the case of the thin section cut

Fig. 17 The simulated fracture process of the CCNBD specimen under mixed mode condition ($\beta = 70^\circ$): minimum principal stress distribution of the central cross section through the notch tip



through the notch tip (Fig. 17), propagating towards the two loading ends. Figure 17 also clearly illustrates that as the mixed mode loading angle β is up to 70° , no self-similar crackings occur at all within the plane of the pre-fabricated chevron notch; and the three-dimensional wing cracking emerges very early in the loading stages.

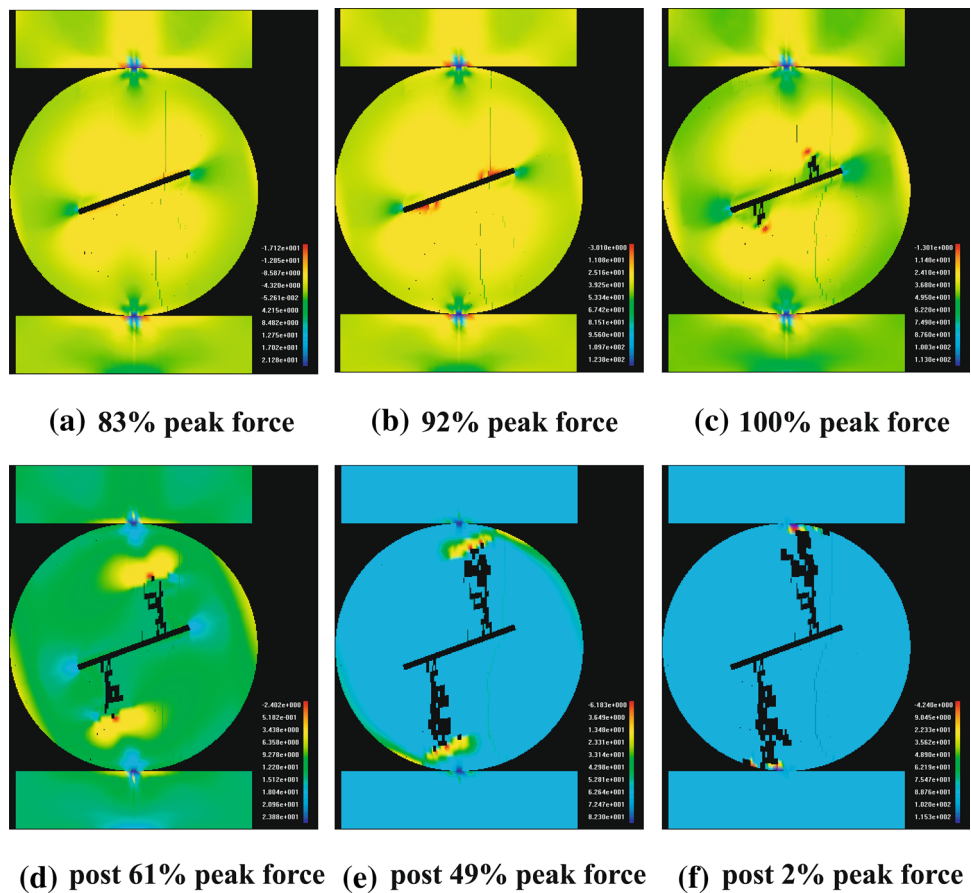
5 Discussions

Core-based rock specimens with pre-fabricated sharp cracks (e.g. CSTBD, SCB) have long been utilized in the literature for fracture toughness tests in different fracture modes involving pure modes I, II and mixed mode. It has been well known that an accurate measurement of the fracture initiation toughness requires sufficient crack tip sharpness for these sample geometries (Kuruppu et al. 2014). For polycrystalline rocks, to ensure reliable measures of fracture toughness, the radius of an intergranular crack shall be comparable to the order of the characteristic material length (e.g. the average grain size in a polycrystalline solid), as evidenced by Lim et al. (1994a, b) on measuring both mode I and mixed mode fracture toughness of a soft rock and later discussed by Dai et al. (2010, 2011)

on measuring fracture toughness of brittle rocks using chevron notched rock samples. For intermediate to coarse grained rocks, these sample configurations are especially convenient for fracture tests due to its ease of sample fabrication; and the interpretation of the crack initiation is straightforward. For fine-grained rocks, pre-cracking is required. However, the sample configurations (e.g. CSTBD, SCB) suffer from the inability to pre-fabricate a sharp straight through crack, which requires tedious pre-cracking treatments prior to tests. Indeed, pre-fabrication of a sharp crack is not easy to perform for brittle solids such as rocks.

The CCNBD specimen for fracture toughness measurements features myriads of merits over other counterparts such as a wide range of specimen geometries that can be tested, higher loading force upon failure, less rock cores required to tests, simple loading fixture and specimen installation. Most importantly, the CCNBD specimen circumvents the difficulty of fabricating sharp cracks by chevron notching rock discs (Fowell 1995). It is commonly believed that the stress concentration at the chevron notched tip triggers the bourgeon of a sharp crack, which further grows in a stable manner by the guidance of the saw-cut notch ligament until the critical crack length is

Fig. 18 The simulated fracture process of the CCNBD specimen under mixed mode condition ($\beta = 70^\circ$): minimum principal stress distribution of the cross section through one quarter thickness



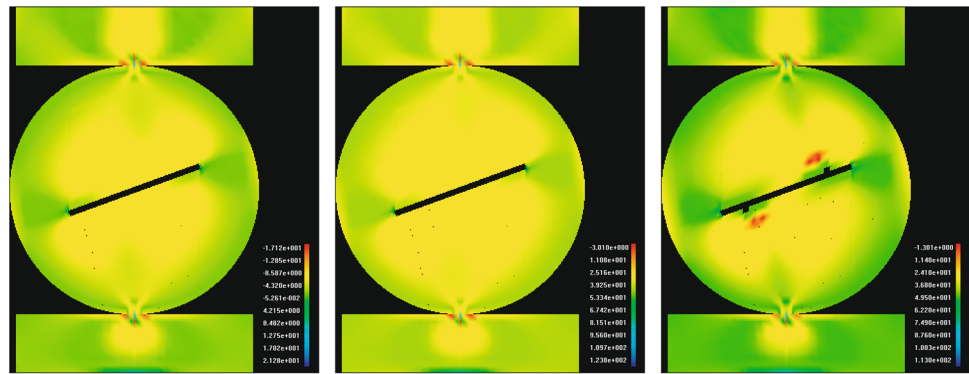
reached during the laboratory experiments. At this critical crack length, as elaborated by Chang et al. (2002), the crack shall become unstable since the further growth of it requires a decreasing load; and thus the mixed mode fracture toughness can be calculated from the instability crack length ($a = a_I$), the corresponding values of N_I and N_{II} as well as the peak loading force recorded from experiments.

However, a comprehensive review by Ayatollahi and Aliha (2008) on the mixed mode experimental results reveals that the scatter in the testing results obtained using CCNBD specimens on Keochang Granite (Chang et al. 2002) and Yeosan Marble (Chang et al. 2002) is significantly higher than those by Awaji and Sato (1978) and Khan and Al-Shayea (2000) using samples with a pre-fabricated straight through crack. Based on the measuring principle (Chang et al. 2002), the crack developed in CCNBD specimen can be divided into two separate stages (Ayatollahi and Aliha 2008). During the first stage, crack initiates from the notch tip and grows stably with a straight crack front; at the second stage, unstable fracture occurs from the straight crack front. For mode I fracture tests using CCNBD, the two stages take place in the same chevron notched plane; however, due to crack kinking in

the mixed mode loading, the fractures at the first and second stages occur in different planes (Ayatollahi and Aliha 2008). Thus, one possible reason for the dramatical scatter in laboratory testing results is the “two-stages” postulation in the CCNBD method adopted for creating the initial crack and growing inside the specimens. Note that when calculating the SIF and the fracture toughness using numerical or analytic methods, a straight through crack propagation (Ouchterlony 1988; Chang et al. 2002) is assumed during the first stage, which is a two-dimensional fracture problem in fracture mechanics. Actually, the two crack fronts of the top and bottom two halves of the rock disc grow along the notched plane to a limited extent depending on the loading angle, but rarely grow up to the root of the notch. The progressive fracture of the CCNBD specimen under mixed mode loading features a typical three-dimensional wing cracking in the linear elastic fracture mechanics.

Our numerical observation of the three-dimensional wing cracking has been evidenced by recent mode II experimental studies (Aliha et al. 2006; Aliha and Ayatollahi 2014), which show that the main fracture emanates from the notch tip and grows somehow along the notched plane of CCNBD specimen but further development of it is

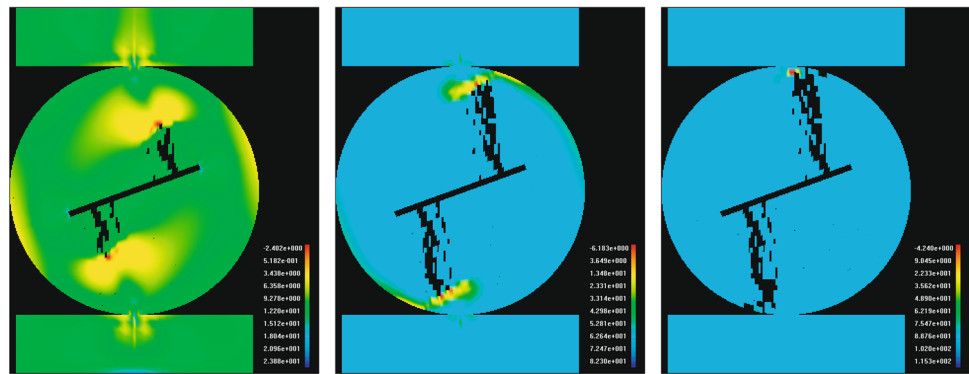
Fig. 19 The simulated fracture process of the CCNBD specimen under mixed mode condition ($\beta = 70^\circ$): minimum principal stress distribution of the cross section through the sample surface



(a) 83% peak force

(b) 92% peak force

(c) 100% peak force

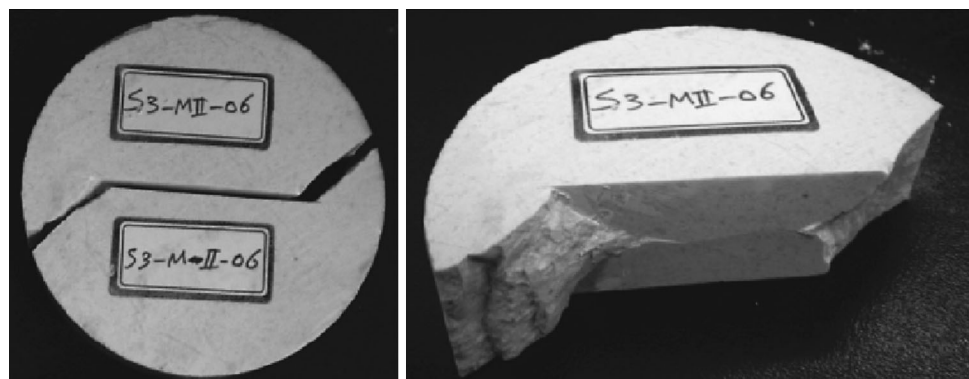


(d) post 61% peak force

(e) post 49% peak force

(f) post 2% peak force

Fig. 20 Photo of a recovered CCNBD sample subjected to pure mode II fracture test (reproduced after Aliha and Ayatollahi 2014) showing the cracks kinking off the chevron notch plane



associated with drastic crack kinking and never reaches the root of the chevron notch (Fig. 20). Although specimen configurations with five mixed mode angles are attempted in our simulations and two typical fracture processes are demonstrated herein, this study stresses that an elaborate investigation on the realistic progressive fracture of the specimen is necessary to assess the measuring principle of the CCNBD specimen subjected to mixed mode loading and to check the validity of the adoption of a straight through crack propagation assumption (Ouchterlony 1988; Chang et al. 2002). The previous treatment can induce

significant errors in calculating the mixed mode SIF and thus inevitable discrepancies in measuring mixed mode fracture toughness as well.

6 Conclusions

The ISRM suggested cracked chevron notched Brazilian disc (CCNBD) specimen for mode I fracture toughness measurement has also been widely utilized to measure the mixed mode fracture toughness of rocks due to its myriads

of advantages over other counterparts. A straight through crack front propagation upon the root of the pre-fabricated chevron notch during the progressive cracking process is assumed in the testing principle but never being rigorously assessed. This study numerically assesses the progressive fracture mechanism of the CCNBD rock specimen under mixed mode loading.

The results show that for CCNBD specimens subjected to mixed mode loading, the very first fracture does initiate from the jag notch tip and grow somehow along the notched plane. However, the primary fracture only grows a little bit within the chevron notched plane and promptly deviates from it, further propagating towards both loading ends. As a result, the primary fracture never reaches the root of the chevron notch as the load reaches its maximum. Further, the saw-cut chevron notch edges of the CCNBD specimen also crack during the progressive failure of the CCNBD under mixed mode loading and thus the generated crack front of the sample is not straight through, but rather curved and twisted. The assumption of a straight through crack propagation (Ouchterlony 1988; Chang et al. 2002) up to the notch root is never satisfied in the realistic rock fracture progress of the CCNBD specimen under mixed mode loading cases. Consequently, the progressive mixed mode fracture of the CCNBD specimen features a typical three-dimensional wing cracking even at the early loading stage. The numerical or mathematical analysis based on the assumption of a straight through crack propagation upon the notch root to determine the mixed mode SIF cannot yield accurate results. In addition, as the mixed mode loading angle is large enough (e.g. 70°), the simulated acoustic emission reveals that the notch tip cracks first and the fracture grows almost vertically toward the loading ends; the primary fracture does not grow at all within the notched plane.

Indeed, due to the existence of the chevron notch, the fracture of the CCNBD specimen under mixed mode loads is a rather complicated three-dimensional issue. Significant errors can be induced by simply adopting the straight through crack propagation assumption and simplifying it as a CSTBD specimen experiencing two-dimensional mixed mode fracturing. The numerical assessment performed in this study depicts a more realistic understanding of the progressive fracture mechanism of the CCNBD specimen which is necessary to more reliably measure the mixed mode fracture toughness of rocks.

Acknowledgments The authors are grateful for the financial support from the program for New Century Excellent Talents in University (NCET-13-0382), the National Program on Key basic Research Project (No. 2015CB057903), National Natural Science Foundation of China (No. 51374149) and the Youth Science and Technology Fund of Sichuan Province (2014JQ0004).

References

- Aliha MRM, Ayatollahi MR (2014) Rock fracture toughness study using cracked chevron notched Brazilian disc specimen under pure modes I and II loading-A statistical approach. *Theor Appl Fract Mech* 69:17–25
- Aliha MRM, Ashtari R, Ayatollahi MR (2006) Modes I and II fracture toughness testing for a coarse grain marble. *Appl Mech Mater* 5–6:181–188
- Aliha MRM, Ayatollahi MR, Smith DJ, Pavier MJ (2010) Geometry and size effects on fracture trajectory in a limestone rock under mixed mode loading. *Eng Fract Mech* 77(11):2200–2212
- Aliha MRM, Ayatollahi MR, Akbaridoost J (2012) Typical upper bound-lower bound mixed mode fracture resistance envelopes for rock material. *Rock Mech Rock Eng* 45(1):65–74
- Alshayea NA, Khan K, Abduljawwad SN (2000) Effects of confining pressure and temperature on mixed-mode (I-II) fracture toughness of a limestone rock. *Int J Rock Mech Min* 37:629–643
- Amrollahi H, Baghbanan A, Hashemolhosseini H (2011) Measuring fracture toughness of crystalline marbles under modes I and II and mixed mode I-II loading conditions using CCNBD and HCCD specimens. *Int J Rock Mech Min* 48(7):1123–1134
- Anderson TL (2005) *Fracture mechanics: fundamentals and applications*. CRC Taylor & Francis, New York
- Atkinson C, Smelser RE, Sanchez J (1982) Combined mode fracture via the cracked Brazilian disk test. *Int J Fract* 18(4):279–291
- Awaji H, Sato S (1978) Combined mode fracture toughness measurement by disk test. *J Eng Mater T ASME* 100(2):175–182
- Ayatollahi MR, Aliha MRM (2007) Wide range data for crack tip parameters in two disc-type specimens under mixed mode loading. *Comput Mater Sci* 38(4):660–670
- Ayatollahi MR, Aliha MRM (2008) On the use of Brazilian disc specimen for calculating mixed mode I-II fracture toughness of rock materials. *Eng Fract Mech* 75:4631–4641
- Backers T, Stephansson O (2012) ISRM suggested method for the determination of mode II fracture toughness. *Rock Mech Rock Eng* 45:1011–1022
- Bažant ZP (2000) Size effect. *Int J Solid Struct* 37:69–80
- Chang SH, Lee CI, Jeon S (2002) Measurement of rock fracture toughness under modes I and II and mixed-mode conditions by using disc-type specimens. *Eng Geol* 66:79–97
- Chen CH, Chen CS, Wu JH (2008) Fracture toughness analysis on cracked ring disks of anisotropic rock. *Rock Mech Rock Eng* 41(4):539–562
- Chong KP, Kuruppu MD (1988) New specimens for mixed mode fracture investigations of geo materials. *Eng Fract Mech* 30:701–712
- Cui ZD, Liu DA, An GM, Sun B, Zhou M, Cao FQ (2010) A comparison of two ISRM suggested chevron notched specimens for testing mode-I rock fracture toughness. *Int J Rock Mech Min Sci* 47:871–876
- Dai F, Xia K (2013) Laboratory measurements of the rate dependence of the fracture toughness anisotropy of Barre granite. *Int J Rock Mech Min* 60:57–65
- Dai F, Chen R, Iqbal MJ, Xia K (2010) Dynamic cracked chevron notched Brazilian disc method for measuring rock fracture parameters. *Int J Rock Mech Min* 47(4):606–613
- Dai F, Xia K, Zheng H, Wang Y (2011) Determination of dynamic rock mode-I fracture parameters using cracked chevron notched semi-circular bend specimen. *Eng Fract Mech* 78(15):2633–2644
- Dai F, Wei MD, Xu NW, Ma Y, Yang D (2015) Numerical assessment of the progressive rock fracture mechanism of cracked chevron notched Brazilian disc specimens. *Rock Mech Rock Eng* 48(2):463–479

- Erarslan N, Williams DJ (2013) Mixed-mode fracturing of rocks under static and cyclic loading. *Rock Mech Rock Eng* 46:1035–1052
- Erarslan N, Liang ZZ, Williams DJ (2012) Experimental and numerical studies on determination of indirect tensile strength of rocks. *Rock Mech Rock Eng* 45(5):739–751
- Fowell RJ (1995) ISRM commission on testing methods: suggested method for determining mode I fracture toughness using cracked chevron notched Brazilian disc (CCNBD) specimens. *Int J Rock Mech Min Sci Geomech Abstr* 32(1):57–64
- Fowell RJ, Xu C (1994) The use of the cracked Brazilian disc geometry for rock fracture investigations. *Int J Rock Mech Min Sci Geomech Abstr* 31(6):571–579
- Funatsu T, Kuruppu M, Matsui K (2014) Effects of temperature and confining pressure on mixed-mode (I–II) and mode II fracture toughness of Kimachi sandstone. *Int J Rock Mech Min* 67:1–8
- Gao X, Shih CF (1998) A parametric study of mixed-mode I/III ductile fracture in tough materials under small scale yielding. *Eng Fract Mech* 60(4):407–420
- Ghazvinian A, Nejati HR, Sarfarazi V, Hadei MR (2013) Mixed mode crack propagation in low brittle rock-like materials. *Arab J Geosci* 6(11):4435–4444
- Haeria H, Shahriarb K, Marjic MF, Moarefvandb P (2014) Experimental and numerical study of crack propagation and coalescence in pre-cracked rock-like disks. *Int J Rock Mech Min* 67:20–28
- Khan K, Al-Shayea NA (2000) Effect of specimen geometry and testing method on mixed I–II fracture toughness of a limestone rock from Saudi Arabia. *Rock Mech Rock Eng* 33(3):179–206
- Kuruppu MD, Obara Y, Ayatollahi MR, Chong KP, Funatsu T (2014) ISRM-Suggested method for determining the mode I static fracture toughness using semi-circular bend specimen. *Rock Mech Rock Eng* 47:267–274
- Liang ZZ, Xing H, Wang SY, Williams DJ, Tang CA (2012) A three dimensional numerical investigation of fracture of rock specimen containing a pre-existing surface flaw. *Comput Geotech* 45:19–33
- Lim IL, Johnston IW, Choi SK, Boland JN (1994a) Fracture testing of a soft rock with semicircular specimens under 3-Point bending.1. Mode-I. *Int J Rock Mech Min Sci Geomech Abstr* 31(3):185–197
- Lim IL, Johnston IW, Choi SK, Boland JN (1994b) Fracture testing of a soft rock with semicircular specimens under 3-point bending. 2. Mixed mode. *Int J Rock Mech Min Sci Geomech Abstr* 31(3):199–212
- Ouchterlony F (1988) ISRM commission on testing methods; suggested methods for determining fracture toughness of rock. *Int J Rock Mech Min Sci Geomech Abstr* 25:71–96
- Shetty DK, Rosenfield AR, Duckworth WH (1985) Fracture toughness of ceramics measured by a chevron-notched diametral-compression test. *J Am Ceram Soc* 68:c325–c443
- Tang CA (1997) Numerical simulation of progressive rock failure and associated seismicity. *Int J Rock Mech Min Sci* 34:249–261
- Tang CA, Kaiser PK (1998) Numerical simulation of cumulative damage and seismic energy release during brittle rock failure—Part I: fundamentals. *Int J Rock Mech Min Sci* 35(2):113–121
- Wang SY, Sloan SW, Tang CA (2014) Three-dimensional numerical investigations of the failure mechanism of a rock disc with a central or eccentric hole. *Rock Mech Rock Eng* 47(6):2117–2137
- Wei MD, Dai F, Xu NW, Xu Y, Xia K (2015) Three-dimensional numerical evaluation of the progressive fracture mechanism of cracked chevron notched semi-circular bend rock specimens. *Eng Fract Mech* 134:286–303
- Weibull W (1939) A statistical theory of the strength of materials. *Ing Vet Ak Handl* 151:5–44
- Whittaker BN, Singh RN, Sun G (1992) *Rock fracture mechanics: principles, design and applications, developments in geotechnical engineering*. Elsevier, Amsterdam
- Xu NW, Tang CA, Li H, Dai F, Ma K, Shao JD, Wu JC (2012) Excavation-induced microseismicity: microseismic monitoring and numerical simulation. *J Zhejiang Univ SCI A* 13(6):445–460
- Xu NW, Dai F, Liang ZZ, Zhou Z, Sha C, Tang CA (2014) The dynamic evaluation of rock slope stability considering the effects of microseismic damage. *Rock Mech Rock Eng* 47:621–642
- Xu NW, Li T, Dai F, Li B, Zhu Y, Yang D (2015) Microseismic monitoring and stability evaluation for the large scale underground caverns of Houziyan hydropower station, southwest China. *Eng Geol* 188:48–67
- Zhou YX, Xia K, Li XB, Li HB, Ma GW, Zhao J, Zhou ZL, Dai F (2012) Suggested methods for determining the dynamic strength parameters and mode-I fracture toughness of rock materials. *Int J Rock Mech Min* 49:105–112